Document donwnloaded from:

[http://hdl.handle.net/20.500.11939/6283]

This paper must be cited as:

[Munera, S., Hernández, F., Aleixos, N., Cubero, S., & Blasco, J. (2019). Maturity monitoring of intact fruit and arils of pomegranate cv.'Mollar de Elche'using machine vision and chemometrics. Postharvest Biology and Technology, 156, 110936.]

ivia
Institut Valencià
d'Investigacions Agràries

The final publication is available at

[http://dx.doi.org/10.1016/j.postharvbio.2019.110936]

Copyright [Elsevier]

Maturity monitoring of intact fruit and arils of pomegranate cv. 'Mollar de Elche' using machine vision and chemometrics

Sandra Munera[a], Francisca Hernández[b], Nuria Aleixos[c], Sergio Cubero[d], José Blasco[e*]

a) Centro de Agroingeniería, Instituto Valenciano de Investigaciones Agrarias (IVIA), Carretera CV-315, Km 10.7, 46113 Moncada, Spain - munera_san@gva.es

b) Grupo de Fruticultura y Técnicas de Producción. Departamento de Producción Vegetal y Microbiología, Universidad Miguel Hernández de Elche, Carretera de Beniel, Km 3.2, 03312 Orihuela, Spain - francisca.hernandez@umh.es

c) Departamento de Ingeniería Gráfica, Universitat Politècnica de València, Camino de Vera, s/n, 46022 Valencia, Spain - naleixos@dig.upv.es

d) Centro de Agroingeniería, Instituto Valenciano de Investigaciones Agrarias (IVIA), Carretera CV-315, Km 10.7, 46113 Moncada, Spain - cubero_ser@gva.es

e) Centro de Agroingeniería, Instituto Valenciano de Investigaciones Agrarias (IVIA), Carretera CV-315, Km 10.7, 46113 Moncada, Spain - blasco_josiva@gva.es (corresponding autor)

Abstract

Pomegranate fruit cv. 'Mollar de Elche' were collected at seven different harvest times. Colour and hyperspectral images of the intact fruit and arils were acquired at each harvest. Physicochemical properties such as total soluble solids, titratable acidity, maturity index, BrimA, internal colour, total phenolic compounds content and antioxidant activity were measured in the juice of each fruit. Relationships between colour (L^*, a^*, b^*) and spectral (720-1050 nm) data obtained from the images of the intact fruit and arils were investigated physicochemical properties using partial least

square regression models. Discrimination of the different maturity stages also was carried out using partial least square discriminant analysis models. Similar results were obtained in the prediction of the physicochemical properties using the colour and hyperspectral images of the intact fruit. However, the predictions achieved for the information about the arils were higher using hyperspectral imaging. In the discrimination of maturity stage, the highest accuracies were obtained using hyperspectral imaging, where 95 % of intact fruit and 100 % of arils where correctly classified. These results indicate the great potential of machine vision techniques, especially hyperspectral imaging, for monitoring the quality of intact 'Mollar de Elche' pomegranate fruit and arils.

Keywords: *Punica granatum; quality; non-destructive; RGB; hyperspectral imaging; NIR;*

1. INTRODUCTION

Pomegranate (*Punica granatum* L.) fruit has gained great importance because it is a source of sugars, organic acids and bioactive compounds (Opara et al., 2009), and has positive health benefits (Viuda-Martos et al., 2010). In Europe, Spain is the largest producer of the fruit, with about 60 % of the total production (65,165 t) (MAPA, 2018) is exported. 'Wonderful', 'Mollar Valenciana' and 'Mollar de Elche' are the most important cultivars (Mena et al., 2011), 'Mollar de Elche' having a sweet taste and soft seeds that make it very much appreciated by consumers and it has its own Protected Designation of Origin.

The commercial quality of pomegranates is based on external attributes such as size, shape and colour (Boussa et al., 2019). However, the colour of the skin does not always indicate its suitability for consumption, and internal attributes such as total soluble

solids (TSS) and acidity also have to be considered to meet market requirements (Fawole & Opara, 2013; Boussa et al., 2019). Since pomegranate is a non-climacteric fruit, it is very important that they are harvested at their proper ripening stage to obtain their highest potential with respect to nutritional, functional and sensory properties (Nuncio-Jáuregui et al., 2014).

The acceptability of the pomegranate by consumers relies on its health benefits and organoleptic properties. Nevertheless, the difficult and time-consuming separation of arils from the rind and membranes limits its consumption. Therefore, consumers are increasingly expressing a preference for packaged ready-to-eat arils and numerous studies have been carried out to evaluate the quality and to develop different strategies to extend the shelf life of this product (Esteve-Peña et al., 2016; Maghoumi et al., 2013; Martínez-Romero, 2013; Özdemir and Gökmen, 2017; Belay et al., 2017).

Qquality control of pomegranate fruit is still performed by traditional methods, mainly because the rind and the arils are delicate and can be damaged by the mechanical operations of machines. Also, production is relatively low and there are no machines that have been properly adapted to such tasks. However, non-destructive techniques are being investigated. For instance, spectroscopy has been investigated to assess the microbial (Adiani et al., 2018) and physicochemical (Arendse et al., 2017; Arendse et al., 2018c) quality in order to detect *Ectomyelois ceratoniae* infestation (Khodabakhshian et al., 2016; Jamshidi et al., 2019), and to predict rind scald (Arendse et al., 2018b). Dielectric spectroscopy has been applied to study the ripeness of this fruit (Castro-Giráldez et al., 2013). A luster sensor has also been employed to measure the glossiness of the rind to determine the quality of intact fruit during storage (Czieczor et al., 2018). Other techniques based on imaging, such as X-rays, have been investigated to quantify the volume of the different parts of the fruit (Salmanizadeh et al., 2014;

Arendse et al., 2016a), and to detect blackheart disease and false codling moth (Arendse et al., 2016b). NMR was used to determine the effect of physiological changes induced by *Alternaria* spp. and *Aspergillus* spp., and to detect blackheart infection (Zhang & McCarthy, 2012) and internal decay (Khoshroo et al., 2009). A computer vision system was developed to sort the arils of automated peeled fruit into different categories depending on the colour (good, immature or rotten arils) in real time (Blasco et al., 2008, 2009). This system was also able to separate raw material from the arils in the commercial line such as pieces of skin or internal membranes coming from the automatic peeling process.

The colour features have been already used to predict physiochemical properties of fruit. Recently, Fashi et al. (2019) related the appearance of the pomegranate with the colours of the arils using image processing. Piedad et al. (2019) used RGB coordinates with machine learning to classify banana tiers in different commercial qualities achieving 97 % of success. Guzman et al. (2015) studied the maturity index of olives using the CIELAB coordinates of the olives. Similarly, Kaur et al. (2018) estimated the maturity of plumps using the RGB coordinates. In this case, high correlations were found between the R/G ratio and TSS. Vidal et al., (2013) used a colour index based on HunterLAB colour coordinates to measure the standard colour of citrus fruits to separate fruits for further degreening processes.

Hyperspectral imaging technology, which integrates both spectral and spatial information (Lorente et al., 2012), has been applied as a powerful analytical processing tool for rapid, non-destructive inspection of the internal and external quality attributes in fruit with thick rind (Arendse et al., 2018a) such as orange (Gomez-Sanchis et al., 2014; Folch-Fortuny et al., 2016), lime (Teerachaichayut & Ho, 2017), or banana (Rajkumar

et al., 2012). However, only Khodabakhshian et al. (2017) have investigated the use of multispectral imaging to determine texture and TSS of intact pomegranate fruit.

The objective of the present study was to evaluate the capability of both machine vision techniques – colour and hyperspectral imaging – to predict the physicochemical properties and the maturity stage of 'Mollar de Elche' pomegranate fruit using the information about both intact fruit and arils.

2. MATERIAL AND METHODS

2.1. Fruit samples

A total of 210 pomegranate fruit cv. 'Mollar de Elche' were collected from a commercial orchard located in San Isidro (Alicante, Southern Spain). Seven harvests were carried out during the 2018 season, from the end of July (90 d after bloom) to the end of October (180 d after bloom), when the fruit were at the full ripeness stage. In each harvest, 30 fruit with no external damage were randomly collected.

In each harvest, all intact fruits were cleaned and weighed and the equatorial diameter was measured. Then, images of all fruit were captured as explained in the next section. After the analysis of the intact fruit, arils were carefully extracted by hand. A total of 20 arils per fruit were randomly selected and the surface moisture was removed by using paper towels. Then, images of the arils were acquired. The rest of the arils were squeezed and the juice thus obtained was used to analyse the chemical properties of each fruit.

From the seven harvesting times, three different maturity stages (immature, half-ripe and ripe) were identified according to the visual features of the intact fruit and the arils (Figure 1).

Figure 1. Example of the appearance of the two opposite sides of intact fruit and arils at each harvest and maturity stage.

2.2 Colour image acquisition and processing

The images were captured using a colour imaging system arranged inside a square inspection chamber consisting of a digital camera (EOS 550D, Canon Inc, Japan) and eight BIOLUX 18W/965 fluorescent tubes (Osram GmbH, Germany) with a colour temperature of 6500 K. Polarising filters were placed in front of the lamps and on the camera lenses to eliminate specular bright spots that could alter the true colour.

The fruit samples were introduced manually upon a holder, and two images were acquired of opposite sides of each intact fruit and one image of the 20 arils on a black background. The images were processed using customised software developed at IVIA (FoodImage-Inspector v4.0, freely available at http//www.cofilab.com) to analyse the colour. First, segmentation was performed. Because of the high contrast between the dark background and the samples, initially a threshold seemed to be sufficient to separate fruit from the background. However, in the case of the darkest fruit or arils, some confusion appeared at the borders and therefore a more sophisticated method was

used. Using this application, regions of interest belonging to a particular class (in this case background and different colours of the samples such as white, reddish or greenish) were selected. Then, using the RGB coordinates of the selected pixels and the class they were assigned to, the software built a discriminant analysis model based on the Bayes theorem. This model allowed any pixel in the image to be classified into one of the predefined classes (background or fruit) as is explained in detail in Blasco et al. (2009). An example of the result of the segmentation is shown in Fig. 2.

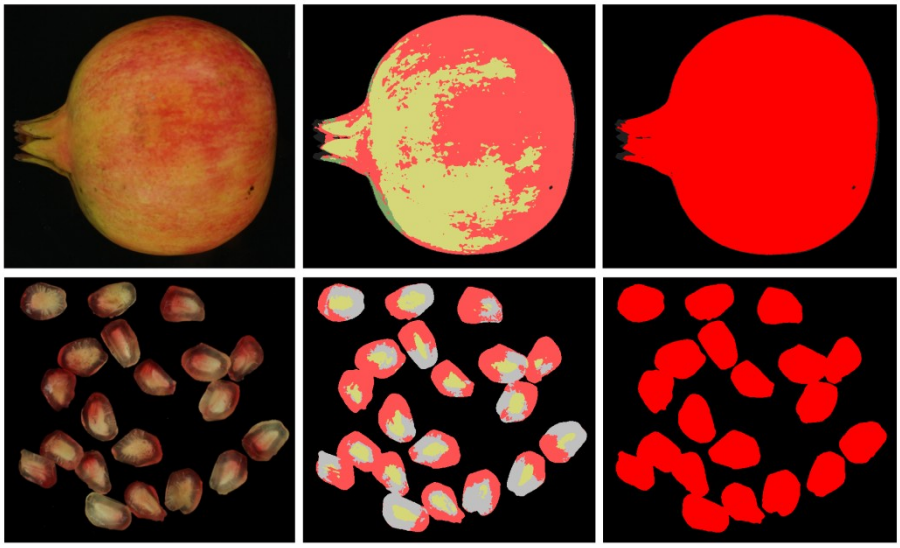

Figure 2. Segmentation of the fruit on the colour images.

The RGB colour coordinates obtained were converted to *L*, a*, b** coordinates (CIELAB colour space), which offer a perception of colour closer to that of the human eye (Blasco et al., 2017). In addition, images of a colour reference target (ColorChecker Digital SG, X-Rite, MI, USA) were also captured as a colour reference. A total of 420 mean *L*, a*, b** values of the intact fruit (two opposite sides) and 210 mean *L*, a*, b** values of arils were extracted.

2.3 Hyperspectral image acquisition and processing

The hyperspectral imaging system was composed of an industrial camera (CoolSNAP ES, Photometrics, AZ, USA), coupled to a liquid crystal tuneable filter (Varispec NIR-07, Cambridge Research & Instrumentation, Inc., MA, USA). The camera was configured to acquire images with a size of 1392 × 1040 pixels and a spatial resolution of 0.14 mm per pixel at 34 different wavelengths every 10 nm, in the working spectral range of 720–1050 nm. In order to avoid problems of unfocused images due to the refraction of light across this wide spectral range, the focus was adjusted on a central band of the acquisition interval and the images were captured using lenses capable of covering the entire spectral range without going out of focus (Xenoplan 1.4/23, Schneider Optics, Hauppauge, NY, USA). To optimise the dynamic range of the camera, prevent saturated images and correct the spectral sensitivity of the different elements of the system, a calibration of the integration time of each band was performed by capturing the average grey level of a white reference target (Spectralon 99 %, Labsphere, Inc, NH, USA) corresponding to 90 % of the dynamic range of the camera.

The scene was illuminated by indirect light from twelve halogen spotlights (37 W) (Eurostar IR Halogen MR16. Ushio America, Inc., CA, USA) powered by direct current (12 V) and arranged equidistant from each other inside a hemispherical aluminium diffuser. The fruit samples were introduced manually into a holder. The inner surface of the aluminium diffuser was painted white to maximise its reflectivity and given a rough texture to minimise directional reflections, which could cause bright spots, the result being a highly homogeneous light.

For the acquisition of the colour, three images per fruit (two of the opposite sides of the intact fruit and one of 20 random arils) were acquired using the hyperspectral imaging system.

The image processing started with the correction of the relative reflectance by using equation (1) (Gat, 2000):

$$\rho_{xy}(x,y,\lambda)=\frac{R^{|\dot{\iota}|}}{R_{\dot{\iota}}^{|\dot{\iota}|}=\rho^{Ref}(\lambda)\frac{R(x,y,\lambda)-R_{\dot{\iota}}(x,y,\lambda)}{R_{\dot{\iota}}(x,y,\lambda)-R_{\dot{\iota}}(x,y,\lambda)}\dot{\iota}}\dot{\iota} \quad (1)$$

Where $\rho^{Ref}(\lambda)$ is the standard reflectance of the white reference target (99 % in this work), $R(x,y,\lambda)$ is the reflectance of the fruit captured by the charge-coupled device (CCD) sensor of the camera, $R_{white}(x,y,\lambda)$ is the reflectance captured by the CCD of the white reference target, and $R_{black}(x,y,\lambda)$ is the reflectance captured by the CCD while avoiding any light source in order to quantify the electronic noise of the CCD.

Later, the background was removed using the clustering based method *k*-means, carried out using the toolbox HYPER-Tools (Mobaraki & Amigo, 2018) for MATLAB R2017b (The MathWorks, Inc. MA, USA) as shown in Figure 3. This method assigns each pixel of the image to the *k* cluster whose centre is nearest, by minimising the sum of the squared distances of each pixel to its corresponding centre (Amigo et al., 2008).

The relative reflectance spectrum of all pixels of each fruit sample was finally extracted, resulting in a total of 420 mean spectra of the intact fruit (two opposite sides) and 210 mean spectra of arils.

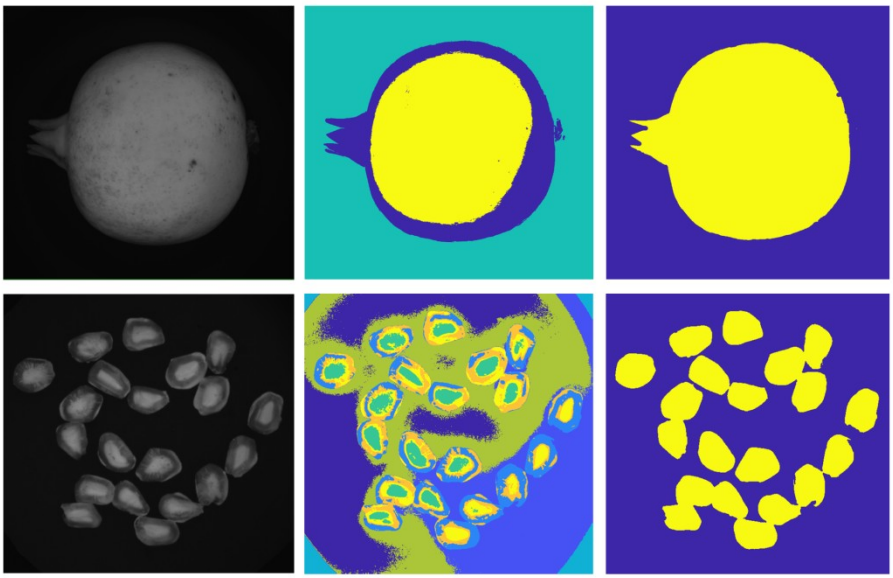

Figure 3. Segmentation of the fruit on the hyperspectral images.

2.4 Chemical properties

2.4.1 Total soluble solids, titratable acidity and maturity indexes

After obtaining the juice of each fruit, the TSS were determined using a digital refractometer (Atago N-20, Atago, Bellevue, Wash., USA) at 20 ºC and results were expressed as %. The TA was determined using an 877 Titrino plus acid-base potentiometer (Metrohm AG, Herisau, Switzerland). The TA results were obtained using 0.1 mol L^{-1} NaOH and expressed as g of citric acid per L. The ratio TSS/TA, or MI, was calculated for each sample. Furthermore, because MI does not always correlate well with the perception of sweetness or sourness in the fruit (Jordan et al., 2001), the BrimA index was also calculated using Eq. (2):

$$BrimA = TSS - k * TA \quad (2)$$

where k is the tongue's sensitivity index ranging from 2 to 10. According to Arendse et al. (2017), a k value of 2 was used to avoid a negative BrimA value.

2.4.2 Total polyphenolic compounds (TPC)

The content of the TPC was determined using the Folin-Ciocalteu method described by Singleton et al., (1999). Absorption was measured at 760 nm using a UV–VIS Spectrophotometer (Helios Gamma model, UVG 1002E, Mercers Row, Cambridge, UK). Calibration curves, with a concentration range between 0 and 0.25 g gallic acid per L, were used for the quantification of TPC, showing a good correlation ($R^2 \geq 0.996$). TPC was expressed as g of gallic acid equivalents L^{-1}.

2.4.3 Antioxidant activity

Following Nuncio-Jáuregui et al. (2015), a methanol extract from each sample was prepared to analyse the antioxidant activity (AA) by mixing 1 mL juice with 10 mL of MeOH/water (80:20, v/v) + 1 % HCl, before sonicating at 20 °C for 15 min and then leaving them for 24 h at 4 °C. The extract was then sonicated again for 15 min, and centrifuged at 25,058 × g for 10 min. The free radical scavenging capacities were determined by three methods, ABTS (Re et al., 1999), DPPH radical (Brand-Williams et al., 1995), and FRAP (Benzie and Strain, 1996). Calibration curves, in the range 0.5 and 5 mmol Trolox L^{-1}, were used to quantify AA, showing a good correlation ($R^2 \geq 0.998$). The absorbance of the three methods was measured using a UV–VIS Spectrophotometer (Helios Gamma model, UVG 1002E, Mercers Row, Cambridge, UK), and the results were expressed as mmol Trolox equivalents L^{-1}.

2.4.4 Data analysis

Finally, one-way ANOVA and multiple-range tests were used to compare the physicochemical parameters in each harvest and maturity stage. The method used to discriminate among the means (Multiple Range Test) was Tukey's procedure. Significance was defined at $p = 0.05$. The groups of samples met the following three

requirements: i) the observations being tested are independent within and among the groups; ii) the groups associated with each mean in the test are normally distributed; and iii) there is equal within-group variance across the groups associated with each mean in the test (homogeneity of variance).

These analyses were performed using StatGraphics software (Manugistics, Inc., Rockville, USA).

2.5. Chemometric methods for quantitative and qualitative analysis

The multivariate data analysis started by partitioning the colour and spectral data of the intact fruit and arils randomly into two sets: two thirds of the samples (training set) were used to calibrate the models and for cross-validation (CV), while the remaining third was used for independent test prediction (test set). In the case of the intact fruit, a total of 280 mean spectra were included in the training set and the other 140 were used in the test set. For the arils, 140 mean spectra were part of the training set and the other 70 were in the test set.

PCA was carried out on the colour and spectral data of the calibration set to obtain an overview of the main source of variance between the samples of different maturity stages. PCA transforms the variables of a dataset into a new set, called the principal components, using linear combinations of the original variables (Basha et al., 2018). This method is usually used for pattern recognition, classification and feature extraction without previous knowledge of the data. The aim of applying PCA was to reduce the dimensionality of the dataset, while retaining most of the variability.

For the quantification of the properties of the samples and discrimination of their maturity, PLS-R and PLS-DA were used. The PLS-R method searches for a linear regression model of latent variables by projecting prediction variables X (colour or

spectral data) and response variables Y (reference properties such as W, D, TSS, TA, MI, BrimA, AA or TPC) into a new latent space where the covariance between these latent variables is maximised. The goal is to find the latent multidimensional direction in the data space that explains the direction of the maximum multidimensional covariance in the reference properties space (Lorente et al., 2012). On the other hand, when the Y variable is categorical, PLS-DA is performed to sharpen the separation between groups of observations by maximising the covariance between the colour or spectral data and the classes, such that a maximum separation among these classes is obtained (Lorente et al., 2012).

To reduce the variability among samples due to light scatter (Rinnan et al., 2009), the mean spectra of the intact fruit and arils were pre-processed using pre-treatments such as SNV and Savitzky Golay derivative (3-point smoothing window, second-order polynomial). Mean centring was applied to normalise the full spectrum.

The selection of the optimal number of LVs, as well as the estimation of the error rate of the PLS-R and PLS-DA models, were performed using a 10-fold CV on the training set (Hastie et al., 2017). In this process, the training set was randomly partitioned into 10 complementary subsets. One subset was used as the validation data for testing the model, and the remaining nine subsamples were used as training data. The cross-validation process was repeated 10 times, leaving one of the subsets out in each iteration of the validation procedure. Finally, the results of the 10 iterations were averaged.

The predictive capability of the PLS-R models was evaluated by the RMSE and the R^2 between the predicted and the measured values of the quality indices for calibration, CV and prediction. Furthermore, RPD, defined as the ratio between the standard deviation of the reference data and RMSEP was also used (Williams, 1987). An RPD

between 1.5 and 2 means that the model can discriminate between low and high values of the response variable. A value between 2 and 2.5 indicates that coarse quantitative predictions are possible, and a value between 2.5 and 3 or above corresponds to good and excellent prediction accuracy, respectively (Williams, 1987). The results of the PLS-DA models were expressed as a percentage of correct classification and total accuracy for calibration, CV and prediction.

3. RESULTS AND DISCUSSION

3.1 Physicochemical changes during maturity

Table 1 summarises the mean and standard deviation of the physicochemical properties measured in the intact fruit and juice samples at each harvest and maturity stage.

The physical properties of the intact fruit such as weight or diameter are important from a commercial viewpoint because these attributes influence consumer preference (Fawole & Opara, 2013). In this case, the W increased from 237 g in the first harvest to 456 g in the last one, while the D increased from 78.9 mm to 95.6 mm. This increase was more noticeable when the fruit passed from the immature to the half-ripe stage. The fruit usually continues growing even after the optimum harvesting time, due to cell expansion from uptake of water and other nutrients (Shwartz et al., 2009). According to the specifications of the 'Granada Mollar de Elche' Protected Designation of Origin (GVA, 2019), fruit weighing less than 125 grams must be excluded.

The TSS increased from 12.0 % in the first harvest to 16.6 % in the last harvest, the values of the last three harvests being non-statistically different. As regards the physical parameters, the increase was more evident when the fruit passed from the immature to the half-ripe stage. This agrees with Nuncio-Jáuregui et al. (2014), who studied three different stages of maturity of 'Mollar de Elche' and obtained TSS values of 14.6, 15.4 and 15.9 %. According to the specifications (GVA, 2019), this indicates that the minimum value of TSS in ripe fruit is 14 %.

Table 1.
Weight (W), diameter (D), titratable acidity (TA), total soluble solids (TSS), maturity index (MI) and BrimA of the pomegranate fruit at each harvest and maturity stage.

	Intact fruit		Juice			
Harvest /	W	D	TSS	TA	MI	BrimA

maturity stage	(g)	(mm)	(%)	(g L^{-1})		
1	$237^{f} \pm 25$	$78.9^{d} \pm 3.1$	$12.0^{e} \pm 1.4$	$2.6^{a} \pm 0.3$	$4.6^{f} \pm 0.3$	$6.7^{e} \pm 1.0$
2	$274^{e} \pm 33$	$82.9^{c} \pm 3.8$	$13.7^{d} \pm 0.9$	$2.5^{ab} \pm 0.1$	$5.5^{e} \pm 0.4$	$8.7^{d} \pm 0.8$
Immature	*$256^{C} \pm 34$*	*$80.9^{C} \pm 4.0$*	*$12.8^{C} \pm 1.4$*	*$2.6^{A} \pm 0.2$*	*$5.1^{C} \pm 0.6$*	*$7.7^{C} \pm 1.3$*
3	$305^{d} \pm 45$	$84.5^{c} \pm 3.8$	$14.8^{c} \pm 0.6$	$2.4^{b} \pm 0.2$	$6.2^{d} \pm 0.5$	$10.0^{c} \pm 0.6$
4	$372^{c} \pm 40$	$90.8^{b} \pm 4.1$	$15.7^{b} \pm 0.8$	$2.2^{c} \pm 0.3$	$7.3^{c} \pm 0.8$	$11.4^{b} \pm 0.8$
5	$423^{b} \pm 64$	$94.8^{a} \pm 3.9$	$16.4^{a} \pm 0.8$	$2.1^{cd} \pm 0.2$	$7.9^{b} \pm 0.5$	$12.2^{a} \pm 0.6$
Half-ripe	*$367^{B} \pm 70$*	*$90.0^{B} \pm 5.8$*	*$15.6^{B} \pm 1.0$*	*$2.2^{B} \pm 0.3$*	*$7.1^{B} \pm 0.9$*	*$11.2^{B} \pm 0.7$*
6	$414^{b} \pm 59$	$93.3^{ab} \pm 4.1$	$16.2^{a} \pm 0.8$	$2.0^{d} \pm 0.3$	$8.4^{a} \pm 1.0$	$12.3^{a} \pm 0.7$
7	$456^{a} \pm 66$	$95.6^{a} \pm 4.1$	$16.6^{a} \pm 0.8$	$2.0^{d} \pm 0.2$	$8.3^{a} \pm 0.6$	$12.6^{a} \pm 0.6$
Ripe	*$435^{A} \pm 66$*	*$94.5^{A} \pm 4.2$*	*$16.4^{A} \pm 0.8$*	*$2.0^{C} \pm 0.2$*	*$8.4^{A} \pm 0.8$*	*$12.5^{A} \pm 0.7$*

Mean value ± standard deviation. Different lowercase letters in the same column means statistical difference between harvests (p-value < 0.05); different capital letters in the same column means statistical difference between maturity stages (p-value < 0.05).

In contrast, TA tended to decrease as maturity progressed. TA of the maturity stages were statistically different, from 2.6 g L^{-1} in immature fruit to 2.0 g L^{-1} in ripe fruit. This trend agrees with Nuncio-Jáuregui et al. (2014), who obtained TA values of 2.5, 2.4 and 2.3 g L^{-1} during maturity. The established minimum value of TA in the ripe fruit of this cultivar is 1.8 g L^{-1} and the maximum is 2.4 g L^{-1} (GVA, 2019).

The MI is commonly used to define the 'taste' of pomegranate fruit during development (Shwartz et al., 2009). The value of MI increased from 4.6 to 8.4 with no statistical difference between the last two harvests. As in the other parameters, the main changes were observed when the fruit passed from the immature to the half-ripe stage. The minimum value of MI in the ripe fruit of this cultivar has to be 6.0 and the maximum 9.0 (GVA, 2019). In this case the value of ripe fruit was 8.4.

Although MI is commonly used, this ratio does not always correlate well with the perception of maturity andJordan et al. (2001) proposed the BrimA index due to the fact

that sugars and acids have opposite effects on flavour, and the tongue is more sensitive to acidity. In this work, BrimA was found to be more related to flavour than MI. The values of BrimA increased from 6.7 to 12.5, with no statistical differences among the three harvests, as in the case of MI.

With regard to the bioactive compounds, Table 2 summarises the mean and standard deviation of the TPC content and the results of the AA measured in the juice samples at each harvest and maturity stage using the DPPH, ABTS and FRAP methods.

Polyphenols have high antioxidant capacity and are also responsible for major organoleptic characteristics, especially colour and taste properties. For this reason, TPC content is an important quality parameter of pomegranate fruit. The TPC content measured in the juice of the fruit in this study decreased from 2.7 to 1.2 g L^{-1}. This decrease was more pronounced in the fourth harvest, the immature fruit being richer in these compounds. Kulkarni and Aradhya (2005) also reported a 55 % reduction in TPC during the initial stage of fruit development and the decrease continued until the fruit was considered fully ripened. Something similar happened with AA, which is related to the level of TPC. The AA decreased from 8.0 to 2.5 mmol Trolox L^{-1} using the DPPH method, from 4.2 to 1.9 mmol Trolox L-1 using ABTS and from 6.4 to 3.1 mmol Trolox L^{-1} using FRAP; this decrease was more pronounced in the fourth harvest. However, these results are different to those obtained by Nuncio-Jáuregui et al. (2014), who presented TPC values of 3.7, 3.3 and 2.7 g L^{-1} and an AA of 7.0, 6.5 and 6.6 mmol Trolox L^{-1} using the DPPH method. As Mena et al. (2011) pointed out, the variation in the concentration of these parameters can vary to a large degree depending on factors such as growing area, weather conditions or the influence of processing techniques such as thinning.

Table 2. Antioxidant activity and total polyphenol content of the pomegranate juice at each harvest and maturity stage. TPC=total polyphenolic compounds.

Harvest time / *maturity stage*	TPC (g L^{-1})	Antioxidant activity (mmol Trolox L^{-1})		
		DPPH	ABTS	FRAP
1	$2.7^{a} \pm 0.3$	$8.0^{a} \pm 0.2$	$4.2^{a} \pm 0.7$	$6.4^{a} \pm 0.9$
2	$2.4^{b} \pm 0.2$	$6.8^{b} \pm 0.4$	$3.8^{b} \pm 0.4$	$5.8^{b} \pm 0.6$
Immature	*$2.5^{A} \pm 0.3$*	*$7.4^{A} \pm 0.7$*	*$4.0^{A} \pm 0.6$*	*$6.1^{A} \pm 0.8$*
3	$2.4^{b} \pm 0.2$	$5.1^{c} \pm 0.7$	$3.9^{b} \pm 0.4$	$6.0^{b} \pm 0.9$
4	$1.2^{c} \pm 0.1$	$3.3^{d} \pm 0.1$	$1.7^{c} \pm 0.2$	$3.0^{cd} \pm 0.5$
5	$1.2^{c} \pm 0.1$	$3.1^{e} \pm 0.2$	$1.6^{e} \pm 0.1$	$2.5^{e} \pm 0.3$
Half-ripe	*$1.6^{B} \pm 0.6$*	*$3.8^{B} \pm 1.0$*	*$2.4^{B} \pm 1.1$*	*$3.8^{B} \pm 1.7$*
6	$1.1^{c} \pm 0.1$	$2.8^{f} \pm 0.2$	$1.8^{c} \pm 0.2$	$2.8^{de} \pm 0.3$
7	$1.2^{c} \pm 0.1$	$2.5^{g} \pm 0.2$	$1.9^{c} \pm 0.2$	$3.1^{c} \pm 0.3$
Ripe	*$1.2^{C} \pm 0.1$*	*$2.7^{C} \pm 0.2$*	*$1.8^{C} \pm 0.2$*	*$3.0^{C} \pm 0.4$*

Mean value ± standard deviation. Different lowercase letters in the same column means statistical difference between harvests (p-value < 0.05); different capital letters in the same column means statistical difference between maturity stages (p-value < 0.05).

3.2 Colour and spectral data analysis

Colour images of intact fruit and arils were acquired in each harvest and the *L**, *a** and *b** colour coordinates were calculated (Figure 4). In the rind, only *a** (which goes from green to red) increased during maturity and all values of the three maturity stages were statistically different. Therefore, the colour of the rind evolved from green to reddish (Figure 1), mainly due to the decrease in chlorophylls and carotenoids content and the increase in the synthesis of pigments such as anthocyanins (Zhao et al., 2015). In the case of arils, the three coordinates evolved during maturity. *L** and *b** (which goes from blue to yellow) decreased, especially from the second to the third maturity stage, while *a** increased greatly. Therefore, the colour of the arils evolved from the immature white arils to reddish (Figure 1) due to the synthesis of anthocyanins (Gil et al., 1995). These changes observed in the colour of the intact frits and arils coincide with those found in the study by Melgarejo et al. (1997).

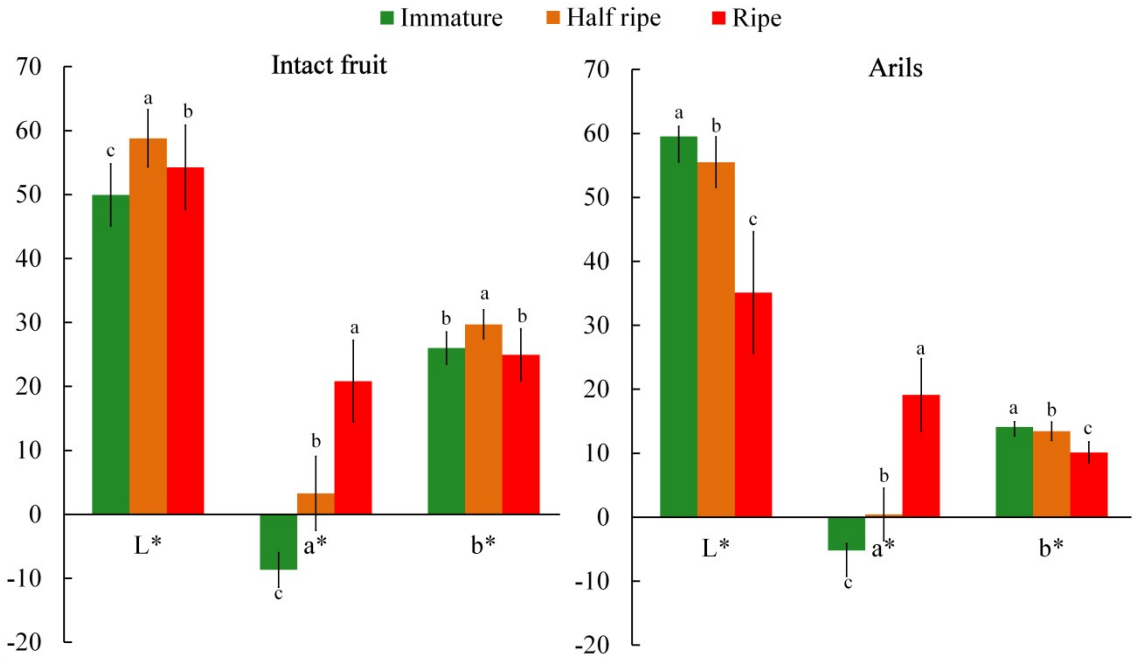

Figure 4. Colour coordinates of the intact fruit and arils at each maturity stage.

The points in the graphic are the mean value and bars are standard deviation. Different letters in the same parameter indicates significant differences between harvests (p-value<0.05), according to Tukey's (HSD) test.

The average mean reflectance spectra obtained from the hyperspectral images for intact fruit and arils are presented in Figure 5. The spectra showed similar trends for intact fruit and arils but the reflectance intensity is different in each maturity stage. This means that they have similar constituents but in different concentrations. In the case of the intact fruit, these differences in reflectance intensity were located around 720–750 nm, close to the chlorophyll absorption peak of 680 nm, and the valley present in the region 960–990 nm, primarily assigned to water absorption bands. This valley was more pronounced in the most mature fruit because the water content increases in the tissues during the onset of ripening, due to cell breakage and osmotic movement of water (Rajkumar et al., 2012).

In the mean spectra of the arils, the differences were more pronounced than in the intact fruit. These were mostly visualised between 720–800 nm, with a peak around 920

404nm and a valley between 960 and 990 nm, assigned to acids, sugars and water
405absorption (Yang et al., 2015). However, as Nicolaï (2007) pointed out, the spectra are
406dominated by the water spectrum with overtone bands of the OH-bonds at 760 nm and
407970 nm, and sophisticated multivariate statistical techniques are needed to extract the
408useful information from these spectra (Cortes et al., 2019).

409

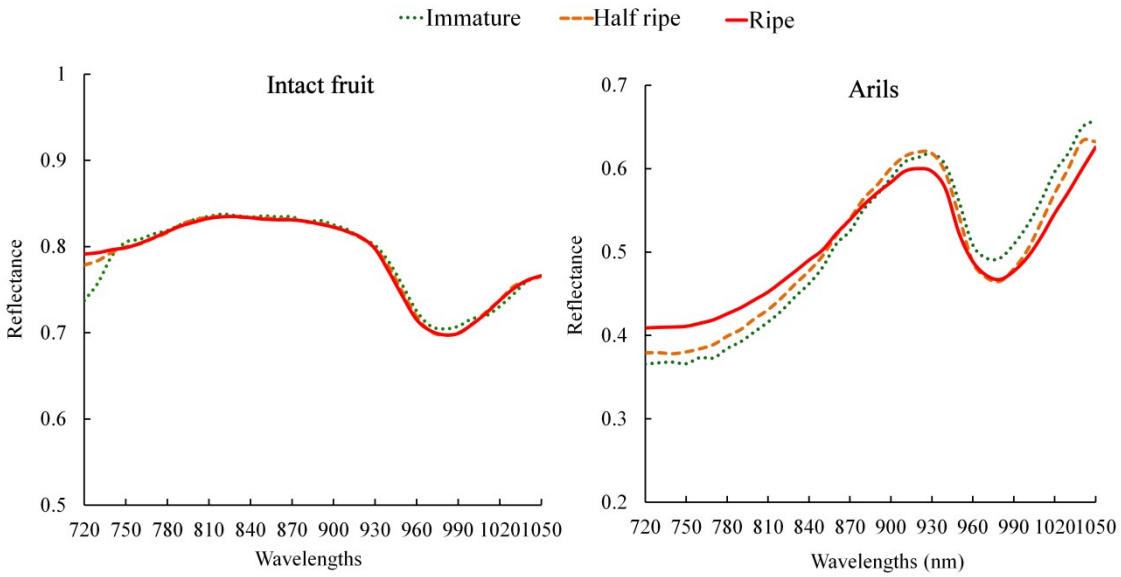

410

411Figure 5. Mean spectra of intact fruit (left) and arils (right) at each maturity stage.

412

413**3.3 Principal component analysis**

414 A PCA was performed to explore the colour and spectral data of the intact fruit and
415arils and to obtain an overview of the distribution of the samples in a non-supervised
416way. Figures 6 and 7 show the score plot and loadings of the PCA using colour and
417spectral data of the intact fruit and arils.

418 Using colour data of the intact fruit, the first two PCs of the model explained 98.5 %
419of the total variance (75.7 % and 22.8 %) and using the data from arils, the first and
420third PCs explained 98.6 % of the total variance (98.1 % and 0.5 %).

In the case of the spectral data of intact fruit, the first two PCs explained 93.6 % of the total variance (84.7 % and 8.9 %) and the first and third PCs explained 85.4 % using the spectral data from arils (84.7 % and 0.7 %).

The scores plot shows the grouping of the fruit in the three maturity stages in all cases. The colour data of the intact fruit shows more separation of the three maturity stages than the spectral data in which the half-ripe and ripe stages were overlapped. This was probably due to the fact that most of the changes that occur during maturity involve pigments that are related to visible wavelengths such as chlorophyll or anthocyanin, among others. The loadings suggest that a^* in the first PC and L^* in the second PC could be the most important colour parameters for the monitoring of maturity in the intact fruit. In the case of the spectral data, although the loadings obtained for PC1 and PC2 might offer information on the most important wavelengths to distinguish the maturity stages, this was not useful since separation was not evident in the score plot.

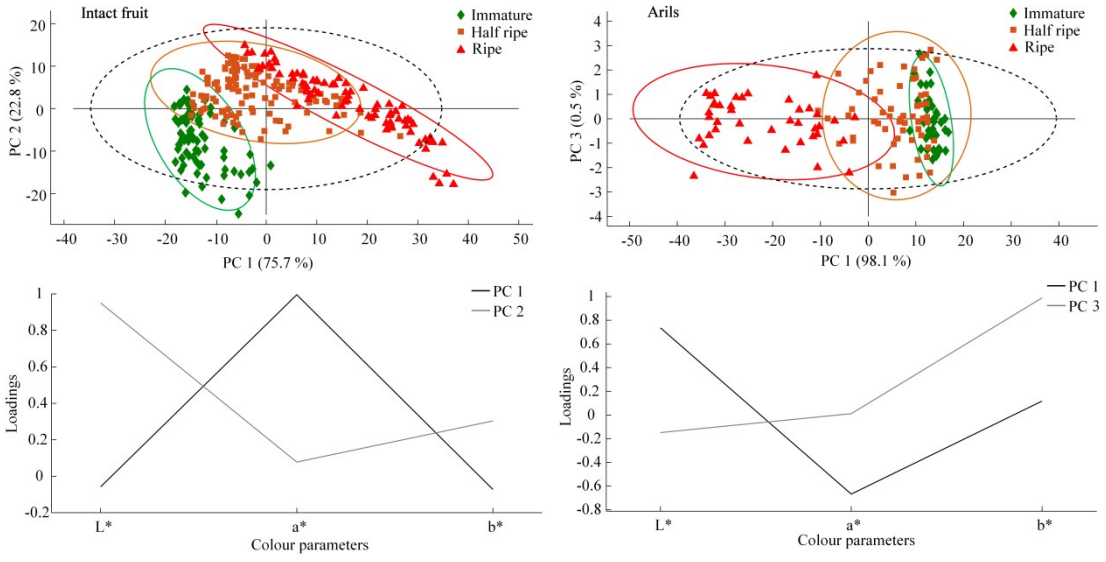

Figure 6. Principal components analysis using colour data. Score plot and loadings of intact fruit (left) and arils (right).

In the case of arils, the best separation of maturity stages was achieved by the spectral data because, in the model based on colour data, immature and half-ripe were overlapped. The corresponding loadings show that although the three colour parameters gave information, this was not sufficient to obtain a clear separation of maturity stages in the score plot. The loadings of the spectral model show that in PC1 the region 960–1050 nm and in PC3 the wavelengths 730, 770, 850, 960 and 980 nm could be the most important wavelengths for the monitoring of maturity in arils.

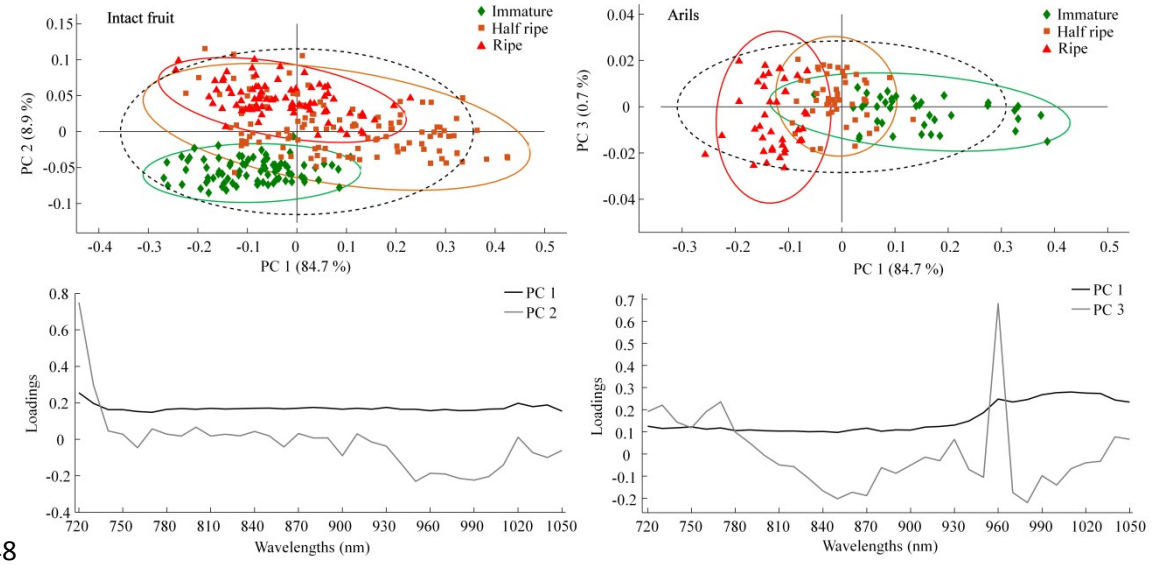

Figure 7. Principal components analysis using spectral data. Score plot and loadings of intact fruit (left) and arils (right).

Although the PCA maximises the variance in the first components, this does not guarantee the separability of data by classes due to its unsupervised nature (Jolliffe, 2002). For this reason, supervised models need to be investigated for use in quantitative and qualitative analyses that are capable of identifying the maturity of the fruit and predicting their physicochemical properties.

3.4. Prediction of the physicochemical properties

Table 3 and 4 show the results of the calibration and validation of the models to predict the physicochemical properties using colour and spectral data of the intact fruit and arils.

Table 3. Results of the prediction of physicochemical properties using the colour data of the intact fruit and arils. #LV=numbers of latent variables; W=weight; D=equatorial diameter; TSS=total soluble solids; TA=titratable acidity; MI=TSS/TA; TPC=total phenolic compounds.

	Property		#LV	Calibration		Cross Validation		Prediction		RPD
				R^2	RMSE	R^2	RMSE	R^2	RMSE	
Intact fruit	W		3	0.65	53.3	0.64	54.0	0.62	58.1	1.6
	D		3	0.67	4.09	0.66	4.14	0.64	4.49	1.6
	TSS		3	0.75	0.94	0.72	0.99	0.68	0.94	1.7
	TA		3	0.53	0.23	0.45	0.24	0.47	0.24	1.4
	MI		3	0.81	0.66	0.81	0.67	0.78	0.70	2.1
	BrimA		2	0.85	0.85	0.84	0.90	0.81	0.92	2.2
	Arils colour	*L**	3	0.78	5.46	0.69	6.51	0.77	5.47	2.1
		*a**	3	0.86	3.95	0.83	4.42	0.85	4.05	2.6
		*b**	3	0.54	1.49	0.47	1.59	0.49	1.44	1.4
	TPC		2	0.82	0.29	0.78	0.32	0.81	0.30	2.3
	DPPH		2	0.89	0.68	0.87	0.74	0.84	0.83	2.5
	ABTS		2	0.77	0.57	0.72	0.62	0.72	0.61	1.9
	FRAP		2	0.71	0.90	0.66	0.98	0.75	0.94	1.9
Arils	TSS		3	0.51	1.32	0.37	1.52	0.44	1.23	1.3
	TA		2	0.41	0.25	0.37	0.26	0.37	0.26	1.3
	TSS/TA		3	0.68	0.87	0.62	0.95	0.55	1.00	1.4
	BrimA		3	0.62	1.37	0.50	1.59	0.53	1.41	1.4
	TPC		2	0.62	0.42	0.51	0.48	0.57	0.45	1.4
	DPPH		2	0.63	1.22	0.48	1.47	0.61	1.28	1.6
	ABTS		2	0.55	0.79	0.43	0.90	0.51	0.80	1.4
	FRAP		2	0.56	1.11	0.45	1.26	0.49	1.30	1.4

Table 4. Results of the prediction of physicochemical properties using the spectral data of the intact fruit and arils. #LV = numbers of latent variables; W=weight; D=equatorial diameter; TSS=total soluble solids; TA=titratable acidity; MI=TSS/TA; TPC=total phenolic compounds.

	Property		#LV	Calibration		Cross Validation		Prediction		RPD
				R^2	RMSE	R^2	RMSE	R^2	RMSE	
Intact fruit	W		9	0.75	45.0	0.71	48.7	0.67	54.2	1.7
	D		5	0.73	3.69	0.70	3.87	0.71	4.10	1.8
	TSS		6	0.80	0.84	0.77	0.90	0.71	0.89	1.8
	TA		4	0.51	0.23	0.48	0.23	0.46	0.24	1.4
	MI		8	0.82	0.64	0.80	0.68	0.71	0.81	1.8
	BrimA		6	0.88	0.78	0.86	0.84	0.85	0.79	2.6
	Arils colour	*L**	7	0.79	5.37	0.70	6.40	0.68	6.45	1.8
		*a**	7	0.83	4.41	0.76	5.22	0.75	5.15	2.0
		*b**	7	0.54	1.49	0.43	1.65	0.45	1.50	1.3
	TPC		9	0.88	0.24	0.84	0.27	0.86	0.25	2.7
	DPPH		5	0.93	0.55	0.91	0.61	0.91	0.62	3.4
	ABTS		9	0.85	0.46	0.81	0.51	0.83	0.47	1.9
	FRAP		9	0.82	0.72	0.78	0.79	0.85	0.74	2.4
Arils	TSS		10	0.82	0.80	0.70	1.07	0.77	0.82	2.0
	TA		5	0.51	0.22	0.34	0.26	0.46	0.24	1.4
	TSS/TA		10	0.83	0.62	0.74	0.78	0.78	0.72	2.1
	BrimA		10	0.89	0.73	0.81	0.97	0.88	0.72	2.7
	TPC		12	0.92	0.19	0.83	0.29	0.87	0.25	2.7
	DPPH		11	0.94	0.48	0.88	0.70	0.92	0.57	3.6
	ABTS		11	0.90	0.37	0.79	0.56	0.81	0.52	2.2
	FRAP		10	0.84	0.66	0.67	0.98	0.76	0.89	2.1

3.4.1 Weight and equatorial diameter

The physical parameters W and D were predicted using only the information of the intact fruit. The models using colour data were calibrated using 3 LVs (Table 3). The R^2 of prediction (R^2_P) was 0.62 and 0.64 with an $RSME_P$ of 58.1 g and 4.49 mm for W and D, respectively. When W and D were correlated with the spectral data, the models were

calibrated using 9 and 5 LVs (Table 4). The R^2_P was 0.64 and 0.71, respectively, and the $RSME_P$ was 54.2 g and 4.10 mm. The results of W prediction using colour and spectral data are in accordance with Arendse et al. (2018c), who obtained an R^2 of 0.62 in the 'Wonderful' pomegranates using Fourier-transform near infrared diffuse reflectance spectroscopy.

Although hyperspectral imaging obtained more accurate results in W and D, the RPD value obtained using colour data was 1.6 for both parameters, and 1.7 and 1.8 using spectral data, respectively. These values indicated that the models can only discriminate the lower from the higher values of the response variable, but this is not sufficient, and hence they are not recommended for a quality control application.

3.4.2 Total soluble solids, titratable acidity and maturity indexes

The models to predict the organoleptic properties such as TSS and TA using the colour data of the intact fruit were calibrated using 3 LVs (Table 3). The R^2_P obtained was 0.68 and 0.47 with an $RSME_P$ of 0.94 % and 0.24 g L^{-1}. In the case of the arils, the models were calibrated using 3 and 2 LVs, respectively (Table 4). The R^2_P obtained was 0.44 and 0.37 with an $RSME_P$ of 1.23 % and 0.26 g L^{-1}. When TSS and TA were correlated with the spectral data, the models using intact fruit information were calibrated using 6 and 4 LVs. The R^2_P was 0.71 and 0.46 and the $RSME_P$ was 0.89 % and 0.24 g L^{-1}. The models using the arils information were calibrated using 10 and 5 LVs, obtaining an R^2_P of 0.77 and 0.46 and the $RSME_P$ was 0.82 % and 0.24 g L^{-1}, respectively.

Other previously tested non-destructive techniques yielded different results in the prediction of these compounds in several cultivars of pomegranate. Arendse et al. (2017) and (2018c) used spectroscopy to predict TSS and TA of 'Wonderful'

pomegranates using the intact fruit information, obtaining an R^2 of 0.78 and 0.77, respectively. Using the aril information they obtained an R^2 of 0.88 and 0.87. Khodabakhshian et al. (2017) predicted the TSS of intact pomegranate fruit cv. Ashraf using a multispectral system and obtained an R^2 of 0.94. Zhang and McCarthy (2013) employed NMR to assess TSS and TA in 'Wonderful' pomegranates, obtaining an R^2 of 0.12 and 0.54.

In this study, the values of RPD obtained for TSS using colour data were 1.7 and 1.3, indicating a fair model performance using intact fruit information but a poor model performance using the information coming from the arils. When the spectral data were used, the values were 1.8 and 2.0, indicating a good model performance using both the intact fruit and the arils information. Thus, quantitative predictions are possible using hyperspectral imaging with intact fruit and arils information. For TA, the RPD value obtained using the intact fruit and arils information and both techniques was 1.4, which indicated a poor performance of the model.

The prediction of MI and BrimA using colour data of intact fruit was performed by means of two models calibrated using 3 and 2 LVs, respectively (Table 3). The R^2_P was 0.78 and 0.81 and the $RSME_P$ was 0.70 and 0.92. Using the colour data from arils, the two models were calibrated using 3 LVs (Table 3). The R^2_P was 0.55 and 0.53 and the RSMEP was 1.00 and 1.41. In the case of spectral data, the R^2_P of MI and BrimA using the intact fruit information was 0.71 and 0.85 and the $RSME_P$ was 0.81 and 0.79 when the models were calibrated using 8 and 6 LVs (Table 4). Using arils information, the R^2_P was 0.78 and 0.88 and the $RSME_P$ was 0.72 when the models were calibrated using 10 LVs (Table 4). Similar results were obtained by Arendse et al. (2018c) in intact 'Wonderful' pomegranates, R^2 of 0.78 and 0.79, and in arils, R^2 of 0.82 and 0.83

(Arendse et al., 2017). Zhang and McCarthy (2013) used nuclear magnetic resonance to assess MI in 'Wonderful' pomegranates, obtaining an R^2 of 0.63.

The values of RPD of MI and BrimA obtained using colour data were 2.1 and 2.2, which indicated a good model performance. However, using the information from the arils, the value of RPD of both indices was 1.4, which indicated a poor performance of the model. The values of RPD using intact fruit were 1.8 and 2.6, indicating a fair model performance for MI and excellent prediction accuracy for BrimA. The values obtained using arils information were 2.1 for the prediction of MI, which means that it is possible to predict this index, and 2.7 for BrimA, indicating an excellent model performance.

The PLS-R models calibrated using the colour data showed a limited potential of TSS, MI and BrimA prediction when the arils information was used. These results demonstrated greater potential of hyperspectral imaging compared to conventional colour imaging for predicting these properties in 'Mollar de Elche' pomegranates using both intact fruit and arils information.

3.4.3 Internal colour

Regarding the internal colour, the prediction models of the colour coordinates of the arils, L^*, a^* and b^*, were predicted using only the information of the intact fruit. The three models using colour data were calibrated using 3 LVs (Table 3). The R^2_P obtained was 0.77, 0.85 and 0.49 and the $RSME_P$ was 5.47, 4.05 and 1.44, respectively. In the case of spectral data, the models were calibrated using 7 LVs (Table 4). The R^2_P was 0.68, 0.75 and 0.45 and the $RSME_P$ was 6.45, 5.15 and 1.50.

The RPD values obtained for L^*, 2.6 and 2.0, indicated an excellent model performance using colour data and a fair model performance using spectral data. The

values obtained for *a**, 2.1 and 1.8, indicated a good model performance using colour data and a fair model performance using spectral data. In the case of *b**, both techniques presented an RPD of 1.4 and 1.3, which means a poor model performance. Arendse et al. (2018c) predicted the *a** coordinate of arils of the 'Wonderful' cultivar using spectroscopy and obtained a similar result to that of hyperspectral imaging: an R^2 of 0.71. These results showed that colour information of the rind had a better correlation with *L** and *a** of arils colour than the spectral data in the NIR region.

3.4.4 Total polyphenolic compounds

In the case of TPC, the models using the colour data of the intact fruit and arils were calibrated using 2 LVs (Table 3). The R^2_P was 0.81 and 0.57 and the $RSME_P$ was 0.30 and 0.45 g L^{-1}. Using spectral data, the model of the intact fruit and arils were calibrated using 9 and 12 LVs (Table 4). The R^2_P was 0.86 and 0.87 and the $RSME_P$ was 0.25 and 0.25 g L^{-1}. Arendse et al. (2018c) and Arendse et al. (2017) also predicted TPC in intact fruit and arils using spectroscopy and obtained similar results to those achieved using hyperspectral imaging: an R^2 of 0.83 using the intact fruit information and 0.87 using the arils information.

The RPD values obtained for colour data were 2.3 and 1.4, indicating a good model performance using the intact fruit information but a poor model performance using arils information. In contrast, the spectral data models obtained a value of 2.7, indicating an excellent performance using both intact fruit and arils information. As in the case of TSS, MI and BrimA, these results demonstrated the greatest potential of hyperspectral imaging for predicting TPC in 'Mollar de Elche' pomegranate using the intact fruit and arils information.

3.4.5 Antioxidant activity

Antioxidant activity was predicted by correlating the values obtained by means of the DPPH, ABTS and FRAP methods, and colour and spectral data of the intact fruit and arils. The three models using the colour data of the intact fruit were calibrated using 2 LVs and the R^2_P was 0.84, 0.72 and 0.75 and the $RSME_P$ was 0.83, 0.61 and 0.94 mmol Trolox L^{-1} (Table 3). The three models using the colour data from arils were also calibrated using 2 LVs but in this case the R^2_P was 0.61, 0.51 and 0.49 and the $RSME_P$ was 1.28, 0.80 and 1.30 mmol Trolox L^{-1}.

When the spectral data of the intact fruit was used, the model for DPPH was calibrated using 5 LVs and the models for ABTS and FRAP were calibrated with 9 LVs (Table 4). The R^2_P was 0.91, 0.83 and 0.85 and the $RSME_P$ was 0.62, 0.47 and 0.74 mmol Trolox L^{-1}. Using the arils information, the models for DPPH and ABTS were calibrated using 11 LVs and the model for FRAP was calibrated using 10 LVs. The R^2_P was 0.92, 0.81 and 0.76 and the $RMSE_P$ was 0.57, 0.52 and 0.89 mmol Trolox L^{-1}.

The RPD values obtained for the DPPH method were 2.5 and 1.6 for colour data, indicating a very good model performance using the intact fruit information and fair model performance using the arils information. Using the spectral data, the RPD values were 3.4 and 3.6, indicating an excellent model performance using spectral data of the intact fruit and arils. In the case of the ABTS method, the value of RPD using colour data was 1.9 and 1.4, which means that the model using intact fruit had a fair performance and a poor model performance using arils information. When spectral data was used, the RPD values were 1.9 and 2.2, which means that the model has a fair and good model performance using the intact fruit and arils information, respectively.

The values obtained for the FRAP method using colour data were the same as with the ABTS method, but 2.4 and 2.1 using spectral data, indicating a good model performance using the spectral data of the intact fruit and arils.

As in the case of TSS, MI, BrimA, and TPC, the PLS-R models calibrated using the colour data showed a limited potential of AA prediction when the arils information was used.

3.5 Classification according maturity stage

Tables 5 and 6 show the calibration and validation results of the models to discriminate the maturity stage using colour and spectral data of the intact fruit and arils.

The model using the colour data of the intact fruit was calibrated using 3 LVs, obtaining a total accuracy of 85.7 % in the CV. In the prediction of the test set, the total accuracy was 84.3 %, in which 80.0 % of immature fruit, 81.7 % of half-ripe fruit and 92.5 % of ripe fruit were correctly classified. In the case of arils, the model was calibrated using 2 LVs, a total accuracy of 85.7 % being obtained in the CV as when the data of the intact fruit were used. In the prediction of the test set, the total accuracy was 85.7 %, in which 85.0 % of immature fruit, 80.0 % of half-ripe fruit and 95.0 % of ripe fruit were correctly classified.

The model using the spectral data of intact fruit was calibrated using 11 LVs, obtaining a total accuracy of 95.0 % in the CV (Table 6). In the prediction of the test set, the total accuracy was also 95.0 %, in which 100 % of immature fruit, 95.0 % of half-ripe fruit and 90.0 % of ripe fruit were correctly classified. When the arils information was used, the model was calibrated using 9 LVs, obtaining a total accuracy of 92.9 % in the CV. In the prediction of the test set, the total accuracy was 100 %, in

626which all fruit were correctly classified into their corresponding classes. These results
627are similar to those obtained using magnetic resonance imaging (Khoshroo et al., 2009),
628but for semi-ripe, ripe and over-ripe fruit (100 %, 98.5 % and 100 %, respectively).

629

630Table 5. Results of classification by maturity stage using the colour data of the intact
631fruit and arils. #LV=number of latent variables; I=immature; HR=half-ripe; R=ripe;
632CC=correct classification; A=accuracy.

	#LV	Class	Calibration			Cross validation			Prediction		
			I	HR	R	I	HR	R	I	HR	R
Intact fruit	3	I	71	11	0	69	12	0	32	6	0
		HR	9	100	3	11	96	5	8	49	3
		R	0	9	77	0	12	75	0	5	37
		CC (%)	88.8	83.3	96.3	86.3	80.0	93.8	80	81.7	92.5
		A (%)		88.6			85.7			84.3	
Arils	2	I	38	10	0	38	11	0	17	5	0
		HR	2	46	3	2	45	3	2	24	1
		R	0	4	37	0	4	37	0	0	19
		CC (%)	95.0	75.0	92.5	95.0	75.0	92.5	85.0	80.0	95.0
		A (%)		86.4			85.7			85.7	

633

634 Although the two machine vision techniques discriminated the maturity stages of the
635intact fruit and arils with good results, hyperspectral imaging was more accurate than
636colour imaging.

637 The results of this study have been confirmed only in fruit of 'Mollar de Elche',
638which is a sweet cultivar of high economic importance in Spain. These experiments
639should therefore be confirmed in other cultivars and with different seasons.

640

641Table 6. Results of classification by maturity stage using the spectral data of the intact
642fruit and arils. #LV=number of latent variables; I=immature; HR=half-ripe; R=ripe;
643CC=correct classification; A=accuracy.

#LV	Class	Calibration			Cross validation			Prediction		
		I	HR	R	I	HR	R	I	HR	R
11	I	80	0	0	80	0	0	40	0	0

Intact fruit		HR	0	116	1	0	110	4	0	57	4
		R	0	4	79	0	10	76	0	3	36
		CC (%)	100	96.7	98.8	100	91.7	95.0	100	95.0	90.0
		A (%)		98.2			95.0			95.0	
Arils	9	I	40	0	0	36	0	0	20	0	0
		HR	0	60	0	3	59	5	0	30	0
		R	0	0	40	0	1	35	0	0	20
		CC (%)	100	100	100	90.0	98.3	87.5	100	100	100
		A (%)		100			92.9			100	

4. CONCLUSIONS

In this work, the potential of colour and hyperspectral imaging has been evaluated to monitor the quality of 'Mollar de Elche' intact pomegranate fruit and arils during maturity.

Different maturity stages could be observed in a non-supervised way by means of PCA using the colour and spectral data of the intact fruit and arils. Later, PLS-R models were performed to predict the physicochemical properties of intact fruit and the arils using the colour and the spectral data (750–1050 nm). The physicochemical parameters that were predicted better (RPD > 2) using colour imaging were the maturity MI and BrimA indices, the L^* and a^* colour coordinates, the AA using the DPPH method and TPC. All of them were performed using the intact fruit information. When hyperspectral imaging was used in the intact fruit, the physicochemical parameters that were predicted better (RPD < 2) were BrimA, a^* colour coordinate, the AA using the DPPH and FRAP methods and TPC. For the arils, all physicochemical parameters studied were correctly predicted (RPD > 2) except TA.

PLS-DA models were performed to classify the fruit according to the maturity stage. The models using colour data were relatively good for intact fruit and arils. However,

when the spectral data were used, more accurate models were obtained with accuracy higher than 95 %.

These findings demonstrate that colour imaging could be used as a potential tool to monitor some physicochemical properties and maturity of the intact fruit. However, hyperspectral imaging has demonstrated a better and greater potential in both intact fruit and arils of 'Mollar de Elche' pomegranate fruit.

Acknowledgements

This work was partially funded by INIA and FEDER funds through project RTA2015-00078-00-00. Sandra Munera thanks INIA for the FPI-INIA grant num. 43 (CPR2014-0082), partially supported by European Union FSE funds.

REFERENCES

Adiani, V., Gupta, S., Ambolikar, R., Variyar, P.S., 2018. Development of rapid method to assess microbial quality of minimally processed pomegranate arils using FTIR. Sensors and Actuators B: Chemical. 260, 800-807. DOI: 10.1016/j.snb.2018.01.095.

Amigo, M.J., Cruz, J., Bautista, M., Maspoch, S., Coello, J., Blanco, M., 2008. Study of pharmaceutical samples by NIR chemical-image and multivariate analysis. Trends in Analytical Chemistry. 27, 696-713. DOI: 10.1016/j.trac.2008.05.010.

Arendse, E., Fawole O. A., Magwaza. L.S. Opara, U.L., 2018a. Non-destructive prediction of internal and external quality attributes of fruit with thick rind: A review. Journal of Food Engineering. 207, 11-23. DOI: 10.1016/j.jfoodeng.2017.08.009.

Arendse, E., Fawole O.A., Magwaza. L.S., Opara, U.L., 2016a. Non-destructive characterization and volume estimation of pomegranate fruit external and internal

687 morphological fractions using X-ray computed tomography. Journal of Food
688 Engineering. 186, 42-49. DOI: 10.1016/j.jfoodeng.2016.04.011.
689Arendse, E., Fawole O.A., Magwaza. L.S., Opara, U.L., 2016b. Estimation of the
690 density of pomegranate fruit and their fractions using X-ray computed tomography
691 calibrated with polymeric materials. Biosystems Engineering. 148, 148-156. DOI:
692 10.1016/j.biosystemseng.2016.06.009.
693Arendse, E., Fawole O.A., Magwaza. L.S., Nieuwoudt, H., Opara, U.L., 2018b.
694 Evaluation of biochemical markers associated with the development of husk scald
695 and the use of diffuse reflectance NIR spectroscopy to predict husk scald in
696 pomegranate fruit. Scientia Horticulturae. 232, 240-249. DOI:
697 10.1016/j.scienta.2018.01.022.
698Arendse, E., Fawole O.A., Magwaza. L.S., Nieuwoudt, H., Opara, U.L., 2018c. Fourier-
699 transform near infrared diffuse reflectance spectroscopy and two spectral
700 acquisition modes for evaluation of external and internal quality of intact
701 pomegranate fruit. Postharvest Biology and Technology. 138, 91-98. DOI:
702 10.1016/j.postharvbio.2018.01.001.
703Arendse, E., Fawole, O.A., Magwaza, L.S., Nieuwoudt, H.H., Opara, U.L., 2017.
704 Development of calibration models for the evaluation of pomegranate aril quality by
705 Fourier-transform near infrared spectroscopy combined with chemometrics.
706 Biosystems Engineering. 159, 22-32. DOI: 10.1016/j.biosystemseng.2017.04.004.
707Basha, N., Nounou, M., Nounou, H., 2018. Multivariate fault detection and
708 classification using interval principal component analysis. Journal of Computational
709 Science. 27, 1-9. DOI: 10.1016/j.jocs.2018.04.017.
710Belay, Z.A., Caleb, O.J., Opara, U.L., 2017. Impacts of low and super-atmospheric
711 oxygen concentrations on quality attributes, phytonutrient content and volatile

712 compounds of minimally processed pomegranate arils (cv. Wonderful). Postharvest
713 Biology and Technology. 124, 119-127. DOI: 10.1016/j.postharvbio.2016.10.007.
714Blasco, J., Cubero, S., Alegre-Sosa, S., Gómez-Sanchis, J., López-Rubira, V., Moltó, E.,
715 2008. Short communication. Automatic inspection of the pomegranate (*Punica*
716 *granatum* L.) arils quality by means of computer vision. Spanish Journal of
717 Agricultural Engineering. 6, 12-16. DOI: 10.5424/sjar/2008061-301.
718Blasco, J., Cubero, S., Gómez-Sanchís, J., Mira, P., Moltó, E., 2009. Development of a
719 machine for the automatic sorting of pomegranate (*Punica granatum*) arils based on
720 computer vision. Journal of Food Engineering. 90, 27–34. DOI:
721 10.1016/j.jfoodeng.2008.05.035.
722Blasco, J., Munera, S., Aleixos, N., Cubero, S., Moltó, E., 2017. Machine vision-based
723 measurement systems for fruit and vegetable quality control in postharvest. Pp 71-
724 91. In: Measurement, modeling and automation in advanced food processing.
725 Advances in Biochemical Engineering/Biotechnology 161. Bernd Hitzmann (Ed.),
726 New York: Springer. DOI: 10.1007/10_2016_51.
727Boussa, F., Zaouay, F., Burlo-Carbonell, F., Nuncio-Jáuregui, N., Gmati, M., El Arbi,
728 B., Melgarejo, P., Hernández, F., Mars, M., 2019. Combined effects of cropping
729 system and harvest date determine quality and nutritional value of pomegranate
730 fruits (*Punica granatum* L. cv. Gabsi). Scientia Horticulturae. 249, 419-431. DOI:
731 10.1016/j.scienta.2019.02.007.
732Brand-Williams, W., Cuvelier, M.E., Berset, C., 1995. Use of free radical method to
733 evaluate antioxidant activity. LWT - Food Science and Technology. 28, 25–30.
734 DOI: 10.1016/S0023-6438(95)80008-5.

735Castro-Giráldez, M., Fito, P.J., Ortolá, M.D., Balaguer, N., 2013. Study of pomegranate
736 ripening by dielectric spectroscopy. Postharvest Biology and Technology. 86, 346–
737 353. DOI: 10.1016/j.postharvbio.2013.07.024.
738Cortés, V., Blasco, J., Aleixos, N., Cubero, S., Talens, P., 2019 Monitoring strategies
739 for quality control of agricultural products using visible and near-infrared
740 spectroscopy: A review. Trends in Food Science & Technology. 85, 138–148. DOI:
741 10.1016/j.tifs.2019.01.015.
742Czieczor, L., Bentkamp, C., Damerow, L., Blanke, M., 2018. Non-invasive
743 determination of the quality of pomegranate fruit. Postharvest Biology and
744 Technology. 136, 74-79. DOI: 10.1016/j.postharvbio.2017.10.008.
745Fashi, M., Naderloo, L., Javadikia, H., 2019. The relationship between the appearance
746 of pomegranate fruit and color and size of arils based on image processing.
747 Postharvest Biology and Technology. 154, 52-57. DOI:
748 10.1016/j.postharvbio.2019.04.017.
749Fawole, O.A., Opara, U.L., 2013. Developmental changes in maturity indices of
750 pomegranate fruit: A descriptive review. Scientia Horticulturae. 159, 152-161. DOI:
751 10.1016/j.scienta.2013.05.016.
752Folch-Fortuny, A., Prats-Montalbán, J.M., Cubero, S., Blasco, J., Ferrer, A., 2016. VIS/
753 NIR hyperspectral imaging and N-way PLS-DA models for detection of decay
754 lesions in citrus fruits. Chemometrics and Intelligent Laboratory Systems. 156, 241-
755 248. DOI: 10.1016/j.chemolab.2016.05.005.
756Gat, N. 2000. Imaging spectroscopy using tunable filters: A review. Technical report,
757 Opto- Knowledge Systems Inc. OKSI.

GVA. 2019. Pliego de condiciones de la denominación de origen protegida “Granada Mollar de Elche". http://www.agroambient.gva.es/va/pc_granadamollarelche. Last accessed June 2019

Gil, M.I., García-Viguera, C., Artés, F., Tomás-Barberán, F.A., 1995. Changes in pomegranate juice pigmentation during ripening. Journal of the Science of Food and Agriculture. 68, 77-81. DOI: 10.1002/jsfa.2740680113.

Gómez-Sanchis, J., Lorente, D., Soria-Olivas, E., Aleixos, N., Cubero, S., Blasco, J., 2014. Development of a hyperspectral computer vision system based on two liquid crystal tuneable filters for fruit inspection. Application to detect citrus fruits decay. Food and Bioprocess Technology. 7, 1047-1056. DOI: 10.1007/s11947-013-1158-9.

Guzmán, E., Baeten, V., Fernandez-Pierna, J.A., García-Mesa, J.A., 2015. Determination of the olive maturity index of intact fruits using image analysis. Journal of Food of Science and Technology. 52, 1462–1470. DOI: 10.1007/s13197-013-1123-7.

Hastie, T., Tibshirani, R., Friedman, J. (2017). Model Assessment and Selection. In The Elements of Statistical Learning: Data Mining, Inference, and Prediction (2nd edition). (pp. 219-257). Springer-Verlag Berlin, Germany.

Jamshidi, B., Mohajerani, E., Farazmand, H., Mahmoudi, A., Hemmati, A., 2019. Pattern recognition-based optical technique for non-destructive detection of *Ectomyelois ceratoniae* infestation in pomegranates during hidden activity of the larvae. Spectrochimica Acta Part A: Molecular and Biomolecular Spectroscopy 206, 552-557. DOI: 10.1016/j.saa.2018.08.059.

Jolliffe, I. T. 2002. Principal component analysis (2nd ed.). New York: Springer.

Jordan, R., Seelye, R., McGlone, A., 2001. A sensory-based alternative to brix/acid ratio. Food Technology. 55, 36–44.

783Kaur, H., Sawhney, B.K., Jawandha, S.K., 2018. Evaluation of plum fruit maturity by
784 image processing techniques. Journal of Food of Science and Technology. 55, 3008-
785 3015. DOI: 10.1007/s13197-018-3220-0.
786Khodabakhshian, R., Emadi, B., Khojastehpour, M. Golzarian, M.R., 2017.
787 Determining quality and maturity of pomegranates using multispectral imaging.
788 Journal of the Saudi Society of Agricultural Sciences16, 322–331. DOI:
789 10.1016/j.jssas.2015.10.004.
790Khodabakhshian, R., Emadi, B., Khojastehpour, M., Golzarian, M.R., 2016. Carob
791 moth, *Ectomyelois ceratoniae*, detection in pomegranate using visible/near infrared
792 spectroscopy. Computers and Electronics in Agriculture. 129, 9-14. DOI:
793 10.1016/j.compag.2016.09.006.
794Khoshroo A., Keyhani A., Zoroofi R.A., Rafiee S., Zamani Z., Alsharif M.R., 2009.
795 Classification of pomegranate fruit using texture analysis of MR images.
796 Agricultural Engineering International: the CIGR Ejournal 11, manuscript 1182.
797Kulkarni, A.P., Aradhya S.M., 2005. Chemical changes and antioxidant activity in
798 pomegranate arils during fruit development. Food Chemistry. 93, 319-324. DOI:
799 10.1016/j.foodchem.2004.09.029.
800Lorente, D., Aleixos, N., Gómez-Sanchis, J., Cubero, S., García-Navarrete, O.L.,
801 Blasco, J., 2012. Recent advances and applications of hyperspectral imaging for
802 fruit and vegetable quality assessment. Food Bioprocess Technology. 5, 1121–1142.
803 DOI: 10.1007/s11947-011-0725-1.
804Maghoumi, M., Gómez, P.A. Mostofi, Y Zamani, Z., Artés-Hernández, F., Artés, F.,
805 2013. Combined effect of heat treatment, UV-C and superatmospheric oxygen
806 packing on phenolics and browning related enzymes of fresh-cut pomegranate arils.
807 LWT - Food Science and Technology 54. 389-396. DOI: 10.1016/j.lwt.2013.06.006.

Manera, F.J., Legua, P., Melgarejo, P., Brotons, J.M., Hernández, F., Martínez, J.J., 2013. Determination of a colour index for fruit of pomegranate varietal group "Mollar de Elche". Scientia Horticulturae. 150, 360–364. DOI: 10.1016/j.scienta.2012.11.036.

MAPA., 2018. Anuario de estadística, Ministerio de Agricultura, Pesca y Alimentación 2017. https://www.mapa.gob.es/estadistica/pags/anuario/2017/anuario/AE17.pdf Last accessed June 2019.

Martínez-Romero, D., Castillo, S., Guillén, F., Díaz-Mula, H.M., Zapata, P.J., Valero, D., Serrano, M., 2013. Aloe vera gel coating maintains quality and safety of ready-to-eat pomegranate arils. Postharvest Biology and Technology. 86, 107-112. DOI: 10.1016/j.postharvbio.2013.06.022.

Melgarejo, P., Martínez-Valero, R., Guillamón, J.M., Miro, M., Amorós, A., 1997. Phenological stages of the pomegranate tree (*Punica granatum* L.). Annals of Applied Biology. 130, 135-140. DOI: 10.1111/j.1744-7348.1997.tb05789.x.

Mena, P., García-Viguera, C., Navarro-Rico, J., Moreno, D.A., Bartual, J., Saura, D., 2011. Phytochemical characterisation for industrial use of pomegranate (*Punica granatum* L.) cultivars grown in Spain. Journal of the Science of Food and Agriculture. 91, 1893-1906. DOI: 10.1002/jsfa.4411.

Mobaraki, N., Amigo, J.M., 2018. HYPER-Tools. A graphical user-friendly interface for hyperspectral image analysis. Chemometrics and Intelligent Laboratory Systems. 172, 174-187. DOI: 10.1016/j.chemolab.2017.11.003.

Nicolaï, B. M., Beullens, K., Bobelyn, E., Peirs, A., Saeys,W., Theron, K.I., Lammertyn, J., 2007. Nondestructive measurement of fruit and vegetable quality by means of NIR spectroscopy: A review. Postharvest Biology and Technology. 46, 99-118. DOI: 10.1016/j.postharvbio.2007.06.024.

833Nuncio-Jáuregui, N., Calín-Sánchez, A., Carbonell-Barrachina, A., Hernández, F.,
834 2014. Changes in quality parameters, proline, antioxidant activity and color of
835 pomegranate (*Punica granatum* L.) as affected by fruit position within tree, cultivar
836 and ripening stage. Scientia Horticulturae, 165, 181-189. DOI:
837 10.1016/j.scienta.2013.11.021.
838Nuncio-Jáuregui, N., Munera-Picazo, S., Calín-Sánchez, A., Wojdyło, A., Hernández,
839 F., Carbonell-Barrachina, A.A., 2015. Bioactive compound composition of
840 pomegranate fruits removed during thinning. Journal of Food Composition and
841 Analysis. 37, 11-19. DOI: 10.1016/j.jfca.2014.06.015.
842Özdemir, K.S., Gökmen, V., 2017. Extending the shelf-life of pomegranate arils with
843 chitosan-ascorbic acid coating. LWT- Food Science and Technology. 76, 172-180.
844 DOI: 10.1016/j.lwt.2016.10.057.
845Peña-Estévez, M.E. Artés-Hernández, F., Artés, F., Aguayo, E., Martínez-Hernández,
846 G.B., Galindo, A., Gómez, P.A., 2016. Quality changes of pomegranate arils
847 throughout shelf life affected by deficit irrigation and pre-processing storage. Food
848 Chemistry 209, 302-311. DOI: 10.1016/j.foodchem.2016.04.054.
849Piedad, E., Larada, J.I., Pojas, G.J., Ferrer, L.V.V., 2018. Postharvest classification of
850 banana (*Musa acuminata*) using tier-based machine learning. Postharvest Biology
851 and Technology. 145, 93-100. DOI: 10.1016/j.postharvbio.2018.06.004.
852Rajkumar, P., Wang, N., EImasry, G., Raghavan, G.S.V., Gariepy, Y., 2012. Studies on
853 banana fruit quality and maturity stages using hyperspectral imaging. Journal of
854 Food Engineering. 108, 194-200. DOI: 10.1016/j.jfoodeng.2011.05.002.
855Rinnan, Å., van den Berg, F., Engelsen, S.B., 2009. Review of the most common pre-
856 processing techniques for near-infrared spectra. Trends in Analytical Chemistry. 28,
857 1201-1222. DOI: 10.1016/j.trac.2009.07.007.

858Salmanizadeh, F., Nassiri, S.M., Jafari, A., Bagheri, M.H., 2014. Volume estimation of
859 two local pomegranate fruit (*Punica granatum* L.) cultivars and their components
860 using non-destructive X-ray computed tomography technique. International Journal
861 of Food Properties. 18, 439-455. DOI: 10.1080/10942912.2013.833521.
862Shwartz, E., Glazer, I., Bar-Ya'akov, I., Matityahu, I., Bar-Ilan, I., Holland, D., Amir,
863 R., 2009. Changes in chemical constituents during the maturation and ripening of
864 two commercially important pomegranate accessions. Food Chemistry. 115, 965-
865 973. DOI: 10.1016/j.foodchem.2009.01.036.
866Singleton, V.L., Orthofer, R., Lamuela-Raventos, R.M., 1999. Analysis of total phenols
867 and other oxidation substrates and antioxidants by means of Folin-Ciocalteu reagent.
868 Methods in Enzymology. 299, 152–178. DOI: 10.1016/S0076-6879(99)99017-1.
869Teerachaichayut, S., Ho, H.T., 2017. Non-destructive prediction of total soluble solids,
870 titratable acidity and maturity index of limes by near infrared hyperspectral imaging.
871 Postharvest Biology and Technology. 133, 20-25. DOI:
872 10.1016/j.postharvbio.2017.07.005.
873Teixeira da Silva, J.A., Rana, T.S., Narzary, D., Verma, N., Meshram, D.T., Ranadeg,
874 S.A., 2013. Pomegranate biology and biotechnology: A review. Scientia
875 Horticulturae. 160, 85–107. DOI: 10.1016/j.scienta.2013.05.017.
876Vidal, A., Talens, P., Prats-Montalbán, J.M., Cubero, S., Albert, F., Blasco, J., 2013. In-
877 line estimation of the standard colour index of citrus fruits using a computer vision
878 system developed for a mobile platform. Food and Bioprocess Technology. 6, 3412-
879 3419. DOI: 10.1007/s11947-012-1015-2.
880Viuda-Martos, M., Fernández-López, J., Pérez-Álvarez, J.A., 2010. Pomegranate and its
881 many functional components as related to human health: a review. Comprehensive

882 Reviews in Food Science and Food Safety. 9, 635–654. DOI: 10.1111/j.1541-
883 4337.2010.00131.x.
884Williams, P.C., 1987. Variables affecting near-infrared reflectance spectroscopic
885 analysis. In: Williams, P., Norris, K. (Eds.), Near-infrared Technology in the
886 Agricultural and Food Industries. American Association of Cereal Chemists, St.
887 Paul, MN, USA, pp. 143-166.
888Yang, C. H., Sun, D.-W., Pu, H., Wang, N.N., Zhu, Z., 2015. Rapid detection of
889 anthocyanin content in lychee pericarp during storage using hyperspectral imaging
890 coupled with model fusion. Postharvest Biology and Technology. 103, 55-65. DOI:
891 10.1016/j.postharvbio.2015.02.008.
892Zhang, L., McCarthy, M.J., 2012. Black heart characterization and detection in
893 pomegranate using NMR relaxometry and MR imaging. Postharvest Biology and
894 Technology. 67, 96–101. DOI: 10.1016/j.postharvbio.2011.12.018.
895Zhao, X., Yuan, Z., Yin, Y., Feng, L., 2015. Patterns of pigment changes in
896 pomegranate (*Punica granatum* l.) peel during fruit ripening. Acta Horticulturae.
897 1089, 83-89. DOI: 10.17660/ActaHortic.2015.1089.9.
898